JACS
JOURNAL OF THE AMERICAN CHEMICAL SOCIETY
pubs.acs.org/JACS
Article

# Computational Design and Theoretical Properties of $WC_3N_6$, an H-Free Melaminate and Potential Multifunctional Material

Da Chen, YiXu Wang, and Richard Dronskowski*

Cite This: https://doi.org/10.1021/jacs.3c00631
Read Online



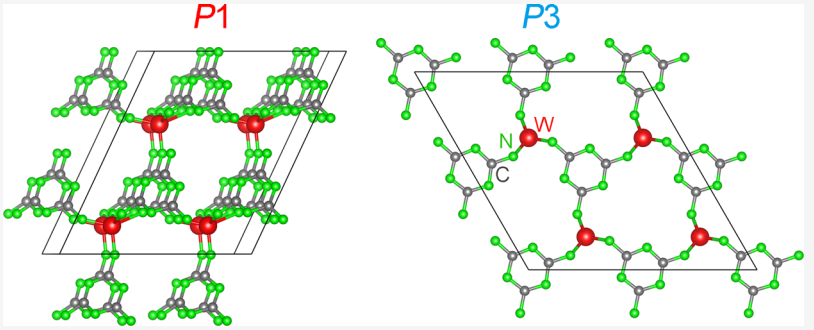


**ABSTRACT:** By means of first-principles theory, existence, synthetic conditions, and structural as well as physicochemical properties have been predicted for the first hydrogen-free melaminate salt of the composition $WC_3N_6$. We find at least two energetically favorable polymorphs adopting space groups *P*1 and *P*3, both of which are layer-like porous materials. In addition to sizable Madelung fields stabilizing saltlike $WC_3N_6$, the complex $C_3N_6^{6-}$ anions are connected via perfectly optimized W−N bonds, forming $WN_5$ in the *P*1 and $WN_6$ coordination polyhedra in the *P*3 polymorphs. The band gaps of the *P*1 and *P*3 phases are HSE-predicted as 2.25 and 1.21 eV, respectively, significantly smaller than those of g-$C_3N_4$ and $WO_3$. Moreover, both phases have suitable band-edge potentials that may provide sufficient driving force for photocatalytic water splitting; at least for the *P*1 phase, there is also a reasonable chance for reduced electron−hole recombination. In addition, the polymorphs's large optical absorption coefficients should greatly enhance the photocatalytic performance. $WC_3N_6$ defines a new class of compounds and has unique structural characteristics, mirrored from its electrical and optical properties, and it should provide another chemical path for preparing efficient photocatalysts and optoelectronic devices.

## INTRODUCTION

Carbon nitride, $C_3N_4$, has fascinated the chemical community for several decades already, starting from the suggested existence and properties[1] and also claimed synthesis and structure,[2] then, however, followed by chemical-bonding theory[3] questioning both existence and composition, in harmony with lessons learned from molecular chemistry.[4] It is probably fair to say that, even now, the ideal composition $C_3N_4$ is almost never reached but, instead, one finds partially amorphous phases of the type $CN_x$ (with $x < 1$), often contaminated with H, O, and also silicon, halogens, and sulfur. Structurally, a great number of polymorphs (graphitic, $Si_3N_4$-like, defect-type ZnS-like, cubic willemite-II-like, and even spinel-like) of $C_3N_4$ have been discussed.[1,5,6] Alternatively expressed, the world is still waiting for convincing single-crystal structure analysis of chemically pure gram-scale $C_3N_4$.

Within more applied research, the so-called "graphitic" carbon nitride dubbed g-$C_3N_4$ made as a two-dimensional species has been suggested as a favorable candidate in the field of photocatalysis due to its unique porous structure, suitable band-edge potentials, as well as chemical and thermal stability.[7] Moreover, g-$C_3N_4$ can be synthesized from various nitrogen-rich precursors such as melamine, dicyandiamide, and methyl ammonium dicyanamide[8] and by various methods, all of which have sparked both experimental and theoretical research.[9] Within g-$C_3N_4$, two important structural and chemical motifs have been highlighted, namely, an infinite extended network structure formed by triazine ($C_3N_3$) or tri-*s*-triazine ($C_6N_7$) units, the two-dimensional nanosheets being held together by van der Waals forces. Density functional theory (DFT) indicates that $C_6N_7$-based g-$C_3N_4$ is the most stable phase under ambient conditions,[9,10] about 30 kJ mol$^{-1}$ more stable than the $C_3N_3$-based g-$C_3N_4$. On the other hand, g-$C_3N_4$ suffers from a few limitations, so it lacks feasibility for wide applications. For example, its band gap is slightly too large,

Received: January 17, 2023

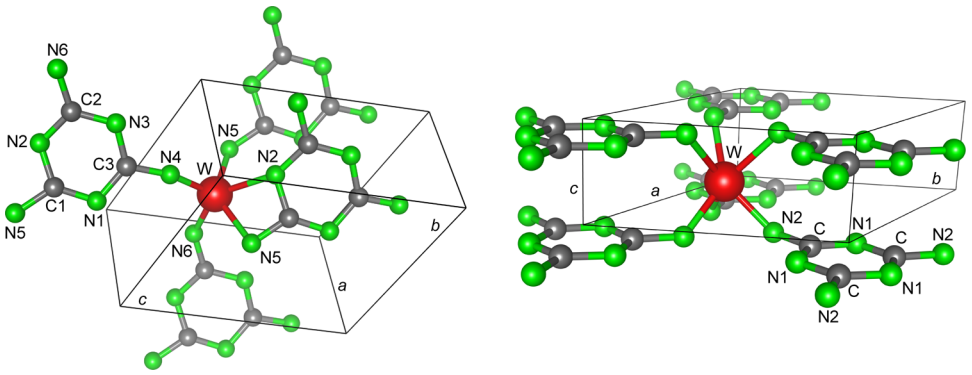


**Figure 1.** Predicted crystal structures of $WC_3N_6$ in space group *P*1 (left) and *P*3 (right).

about 2.7−2.8 eV,[7,11,12] which reduces its visible light absorption threshold to 460 nm, thus limiting the photocatalytic performance. Further research indicates that metal ions might modulate the porous structure of carbon nitride, lower its band gap, assist in separating photogenerated carriers, and enhance conductivity.[13−18]

Besides binary $C_3N_4$, carbon−nitrogen-based complex anions such as carbodiimide[19−24] $NCN^{2-}$, guanidinate[25,26] $CN_3^{5-}$, or ortho-nitrido carbonate[27] $CN_4^{8-}$ also allow to generate three-dimensional materials in combination with (transition) metal cations, and these may be regarded as complex *salts* offering rich structural diversity and physicochemical properties. Molecular melamine, $C_3H_6N_6$, the trimer of molecular cyanamide, $H_2NCN$, plays a special role not only because it may be used for making g-$C_3N_4$ (see above) but also due to the fact that it allows for deprotonation to prepare metal melaminate salts,[28−30] yet another way to arrive at high-performance photocatalysts. In fact, the literature provides recent examples for synthesis and structural characterization (by means of single-crystal XRD) of highly interconnected, multi-coordinated melaminate salts by deprotonation with potassium, rubidium, and copper.[31,32] When carried out in liquid ammonia, only the singly deprotonated K/Rb melaminates precipitate because even $NH_3$ is insufficiently basic for full deprotonation. For Cu melaminate, a metathesis arrives at triple deprotonation without any solvents. On the basis of above studies, we wondered whether melamine could be *completely* deprotonated to achieve a hydrogen-free melaminate salt involving more powerful metathetic conditions. In what follows, we present the result of a computational study from first principles aiming at such phase dubbed $WC_3N_6$ and its chemical as well as physicochemical properties. Two polymorphs of $WC_3N_6$ are likely to exist, and their electronic band gaps and band-edge potentials indicate applicability in the fields of photocatalysis, optoelectronic devices, and possibly more.

**Calculation Details.** First-principles structural searches for the $WC_3N_6$ composition were performed through a particle swarm optimization algorithm implemented in the CALYPSO code,[33−35] which, just like USPEX,[36−38] is an established structure-prediction method.[39,40] The structural search used a cutoff energy of 400 eV and a *k*-point spacing of 0.35 $Å^{-1}$. The "molecular" module was employed by assembling the crystal structure from W atoms and $C_3N_6$ units, with structural models containing one, two, and four formula units. The search stopped after reaching convergence, each with approximately 1000 structures generated; only the "fourfold" search failed to arrive at reasonable structures. The structure optimizations were conducted using the Perdew−Burke−Ernzerhof (PBE)[41] functional augmented with dispersion corrections by the D3 (BJ) approach[42,43] utilizing the VASP code[44−47] together with PAW pseudopotentials.[48,49] A plane-wave energy cutoff of 500 eV and a *k*-point spacing of 0.3 $Å^{-1}$ were used to ensure energetic convergence. Additional electronic-structure calculations were performed using three different functionals, PBE, PBE + $U$[50] ($U$ = 2.2,[51] 6.2,[52] and 9 eV,[53] based on the reference values suggested in previous studies), and HSE06.[54] The absorption spectra were calculated using the HSE06 + RPA method with a plane-wave energy cutoff of 500 eV and a *k*-point spacing of 0.3 $Å^{-1}$ after the convergence test. Previous studies indicate that the method of directly calculating the band-edge potentials from Sanderson's electronegativity method can be well applied to systems such as transition metal oxides, but not to the $C_3N_4$ system.[55] We therefore used a standard method to obtain the band-edge positions of $WC_3N_6$ by calculating the absolute vacuum level.[56] Molecular dynamics simulations were carried out using *NVT* ensembles with a time step of 1 fs at 300 and 600 K. The chemical bonding was analyzed by calculating Crystal Orbital Hamilton Populations (COHP) and their integrals (ICOHP), fat bands, overlap-matrix elements, wavefunction-based Löwdin charges, and Madelung energies based on the latter using LOBSTER 4.1.0.[57−62] Brillouin zone paths, band structures, and optical absorption spectra were generated with the aid of VASPKIT.[63] The crystal structures were visualized using VESTA.[64]

## RESULTS AND DISCUSSION

Because a fully deprotonated melamine anion (melaminate) will carry a charge of −6, a counter cation such as $W^{6+}$ is self-explanatory, and this maximum oxidation state of tungsten is easy to achieve.[65] An extensive structure search for $WC_3N_6$ arrives at two crystal structures with space groups *P*1 (triclinic system, structural parameters in Table S1) and *P*3 (trigonal system, Table S2) with favorable energies; we will use their space groups to designate them in what follows. Additional structural candidates with higher energies are found in Table S3 but are not discussed any further. The *P*1 phase of $WC_3N_6$ is more stable than *P*3 by about 96 kJ $mol^{-1}$ (PBE+D3) but *P*3 may still be a favorable candidate depending on the synthetic route, as also shown for the $C_3N_4$ system.[9] Note that, for large enough energetic barriers, metastable structures are likely to form according to Ostwald's step rule.[66]

Figure 1 offers views into the crystal structures of the *P*1 and *P*3 polymorphs of $WC_3N_6$. Phonons and molecular dynamics


https://doi.org/10.1021/jacs.3c00631
J. Am. Chem. Soc. XXXX, XXX, XXX−XXX

calculations confirm the stability of these structures; see Figures S1 and S2.

Both *P*1 and *P*3 polymorphs contain individual melaminate anions bonded to tungsten cations, and both polymorphs are layer-like and also contain pores; at the same time, their saltlike ionic character is confirmed from significant Madelung energies, −2899 and −2574 kJ mol$^{-1}$ for *P*1 and *P*3, although covalency also plays an important role (see below). In the *P*1 polymorph, the central W atom is subject to a rather irregular 4 + 1 coordination by nitrogen, with interatomic W−N distances of 1.78, 1.83, 1.99, 2.10, and 2.17 Å (Figure 1, left). This yields an average W−N distance of 1.97 Å, which perfectly fits the sum of the ionic radii of $W^{6+}$ (0.51 Å for fivefold coordination) and $N^{3-}$ (1.46 Å),[67] so the ionic character is also mirrored from the distances. The other polymorph dubbed *P*3 (Figure 1, right) is predicted to show structural similarities to g-$C_3N_4$.[7] Here, the W atom bonds to nitrogen atoms in the form of an approximate trigonal prism (CN = 3 + 3), and the W−N distances are 1.97 (3×) and 2.13 (3×) Å, averaged 2.05 Å. With an $W^{6+}$ ionic radius of 0.60 Å for sixfold coordination, the expected W−N bond length is 2.06 Å, extremely close to the prediction.

To synthetically realize the $WC_3N_6$ phase, we propose a metathetic path according to

$$WO_{3(s)} + C_3H_6N_{6(s)} = WC_3N_{6(s)} + 3\,H_2O_{(g)}$$

involving three solids ($WO_3$, $C_3H_6N_6$, $WC_3N_6$) and gaseous $H_2O$, as illustrated from the Gibbs energy shown in Figure 2. Clearly, generating water as a reaction product is the essential driving force to provide sufficient thermodynamics for $WC_3N_6$ phase formation.

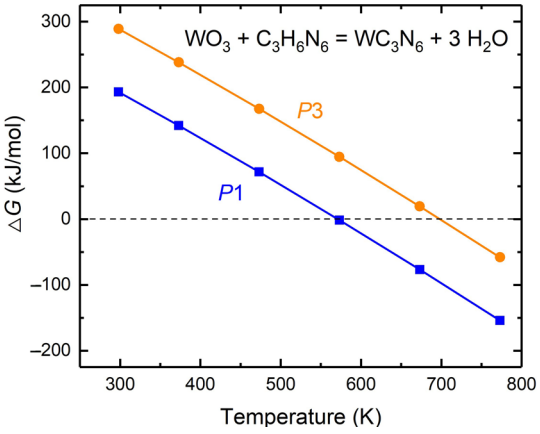


**Figure 2.** Gibbs energy of the $WC_3N_6$ synthesis as a function of temperature.

For first calculating the energetics at absolute zero temperature, we took the $P2_1/n$ phase of $WO_3$,[68] the $P2_1/a$ phase of $C_3H_6N_6$,[69] and the $P6_3/mmc$ phase of $H_2O$.[70] Including the entropic contribution of gaseous $H_2O$ at a finite temperature, thereby approximately reaching Gibbs energies, was based on $H_2O$ gas-phase thermochemical data[71] and neglecting the (small) finite-*T* energy-free enthalpy difference of the solids. At about 570 K (697 K), easily achieved in any laboratory, the reaction already becomes exergonic for the *P*1 (*P*3) phase, more than 200 °C (70 °C) lower than the synthetic temperature of g-$C_3N_4$ formation[9] if starting with melamine. In addition, it is quite encouraging that the calculated formation enthalpy of $WC_3N_6$ shown in Figure S3 confirms the thermodynamic stability against decomposition into $C_3N_4$ and $WN_2$, the most likely (or existing) competing phases at standard pressure.

With regard to the aforementioned covalent contributions, the chemical-bonding analysis was carried out based on LOBSTER;[57−62] see Figure 3. The COHP plot of the W−N bonds (Figure 3, left) demonstrates that there are almost no antibonding levels in the valence region, in contrast to the unoccupied conduction bands, so covalency is nicely optimized. With regards to the absolute numbers by integrated COHP (Figure 3, right), all W−N bonds together in *P*1 are about 0.8% stronger than those of *P*3, so the five slightly shorter W−N bonds exceed the six longer W−N bonds in strength. The C−N bonds, however, are 1.0% stronger in the *P*3 phase than in the *P*1 phase, and they are very similar to those in molecular melamine.

Another detail relates the total ICOHP over all W−N and C−N bonds, and here, *P*1 comes out a little (0.6%) smaller than *P*3, so the more stable and more ionic (by Madelung energy, see above) *P*1 phase is slightly less covalent than *P*3, also mirrored from the volume which is larger for *P*1 than for *P*3 (81 vs 72 cm$^3$ mol$^{-1}$), almost coinciding with the molar volume of molecular melamine[72] (79 cm$^3$ mol$^{-1}$); note that the volume increments of $H^+$ and $W^{6+}$ are zero,[73] that is to say that the larger volume of *P*1 indicates less overlap and less covalency in *P*1. Consequently, the ionicity of *P*1 is stronger, as reflected from the wavefunction-based Löwdin charges, see Table S4, and, hence, the electrostatic Madelung energies based on these charges, as mentioned before. It does not come as a surprise that the more ionic *P*1 polymorph with a larger volume, larger charges, and larger Madelung energy also has a larger band gap than the *P*3 polymorph (see Figure 4). This implies that one can modulate a material's band gap to some extent by adjusting its coordination and, hence, volume, and similar observations have been made before in the field of high-pressure chemistry.

Since the PBE functional[41] has not been made for calculating reasonable band gaps of semiconductors, we study the band structure of $WC_3N_6$ with alternative methods. Both PBE and PBE + *U*[50] underestimate the band gap compared to the Heyd−Scuseria−Ernzerhof (HSE06) hybrid functional,[54] among which PBE + *U* (*U* = 9 eV) comes closest to HSE06; see Table S5.

As seen in Figure 4, both *P*1 and *P*3 polymorphs are indirect semiconductors with band gaps of 2.25 and 1.21 eV, respectively, significantly smaller than those of g-$C_3N_4$ and $WO_3$,[7,11,12,74] so there is potential in fabricating high-efficiency optoelectronic devices. The valence band maximum (VBM) of *P*1 locates at $\mathbf{U}_2$ while its conduction band minimum (CBM) appears at $\mathbf{T}_2$. Interestingly, the direct transition at $\mathbf{V}_2$ (2.43 eV) is smaller than that at $\mathbf{U}_2$ (2.50 eV) and $\mathbf{T}_2$ (2.54 eV), and it is 0.18 eV larger than the indirect gap, 2.25 eV between $\mathbf{U}_2$ and $\mathbf{T}_2$. As for the *P*3 polymorph, the VBM and CBM occur at **Z** and **X**, respectively. The direct transition at **X** (1.30 eV) is smaller than that at **Z** (1.74 eV), and it is only 0.09 eV larger than the indirect gap, 1.21 eV between **Z** and **X**. Therefore, the *P*3 polymorph can be regarded as a quasi-direct gap semiconductor, similar to g-$C_3N_4$.[11]

As expected from the COHP analysis of $WC_3N_6$, the DOS given in Figure S4 proves that the VBM of *P*1 mainly originates from nitrogen p orbitals while the CBM is mostly formed by tungsten d orbitals and also nitrogen p orbitals, accompanied


https://doi.org/10.1021/jacs.3c00631
J. Am. Chem. Soc. XXXX, XXX, XXX−XXX

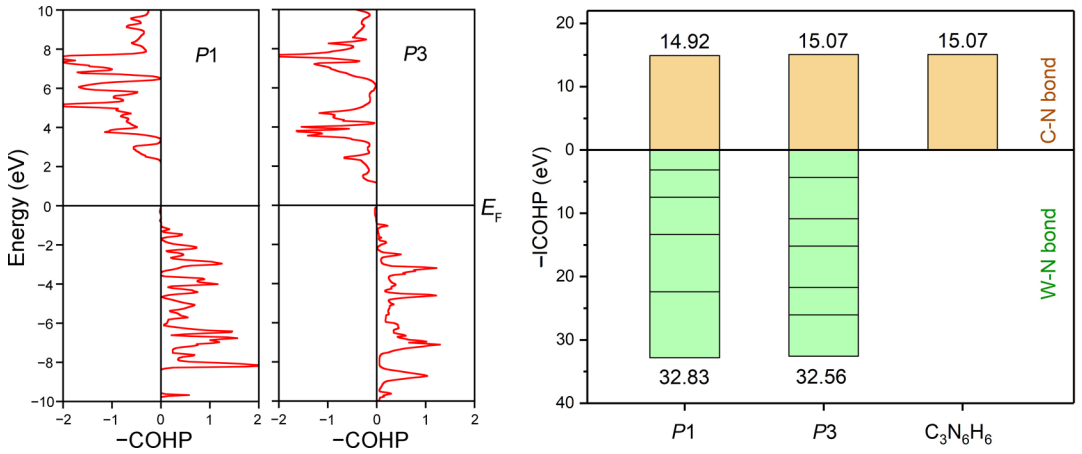


**Figure 3.** Chemical-bonding analysis of $WC_3N_6$ as seen from COHP analysis (left) and ICOHP data (right). As given on the left, the averaged COHP of the W−N bonds in both *P*1 and *P*3 polymorphs are practically devoid of antibonding up to the Fermi level, thereby mirroring perfectly optimized covalency. On the right, the ICOHP data of the W−N bonds (green) arrive at about the same bond energy in both polymorphs (*P*1 being slightly stronger), and the energy of the averaged C−N bonds (orange) is also very similar to the one in melamine.

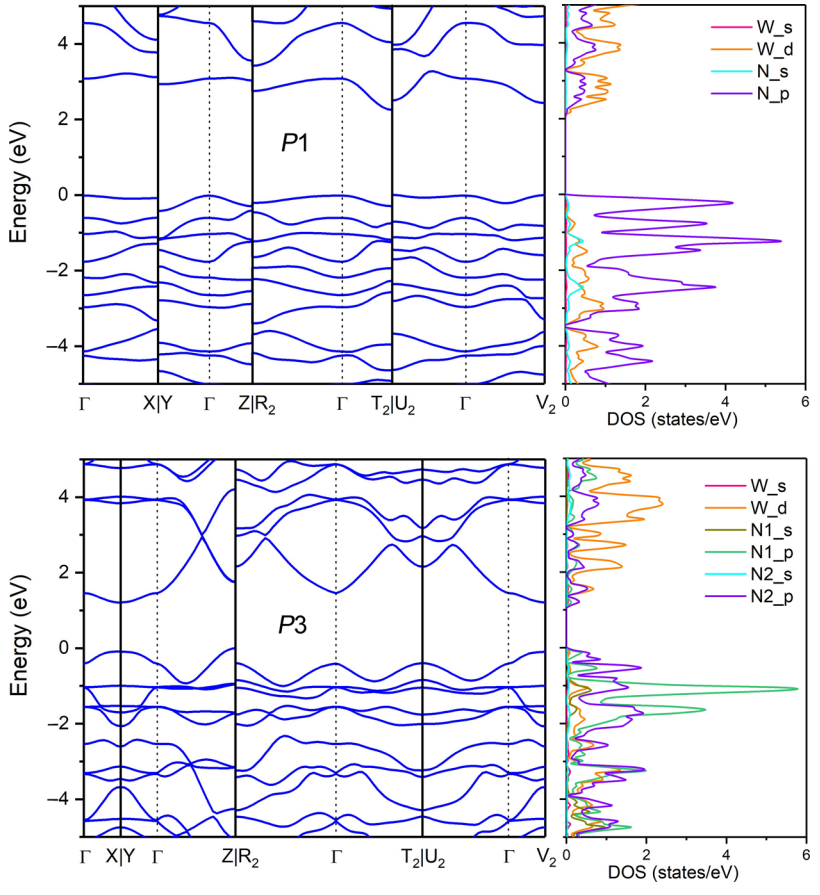


**Figure 4.** Band structure and density of states (DOS) of $WC_3N_6$ calculated by using the Heyd−Scuseria−Ernzerhof (HSE06) hybrid functional for the *P*1 (top) and *P*3 (bottom) polymorphs.

by a minority carbon p contribution. A similar situation is found in *P*3, and here, the contribution from carbon p orbitals is almost zero. For the convenience of analysis, the DOS diagram in Figure 4 has been drawn only including the contributions from W and N atoms. The terminal N2 p orbitals in the *P*3 phase contribute more to the CBM and VBM than those of the inner N1 atoms, a trivial finding because W directly bonds to N2. To further study the electronic transition between CBM and VBM, we also calculated the fat bands and all overlap-matrix elements using LOBSTER. Figure S5 proves that the energetic transition of photogenerated electrons in *P*1 is mainly from nitrogen (N4, N5 and N6) p to tungsten d orbitals, and the maximum overlap between these two kinds of orbitals is only 0.25; while this does not strictly indicate noncoplanarity with regard to N and W orbitals, it is rather small and should therefore improve separating photogenerated carriers and photocatalytic performance.[75] As for *P*3, the energetic transition of photogenerated electrons is mainly from


https://doi.org/10.1021/jacs.3c00631
J. Am. Chem. Soc. XXXX, XXX, XXX−XXX

nitrogen (N2) p to tungsten d orbitals and also a small part of nitrogen (N2) p orbitals. Here, the maximum overlap between N2-2p and W-5d orbitals is only 0.23, a good sign, but the existence of N2-2p (*full* orbital overlap between CBM and VBM) may inhibit charge separation.

Due to tungsten's large nuclear charge, studying the influence of spin-orbit coupling on the band structure of $WC_3N_6$ is required (see Figure S6), but the effect is quenched within the valence band due to strong orbital interactions, although it is apparent for the conduction band and leads to band splitting. In addition, the valence band is nitrogen-like and the conduction band tungsten-like; see Figure 4.

Apart from favorable band gaps, suitable band-edge potentials are also crucial for photocatalysis. For the water-splitting reaction, the CBM must be higher than the $H^+/H_2$ level of water reduction (−4.44 eV + pH × 0.059 eV), whereas the VBM must be lower than the $H_2O/O_2$ level of water oxidation (−5.67 eV + pH × 0.059 eV); otherwise, water splitting is energetically unfeasible without an external bias voltage.[22,27,76,77] The band-edge positions relative to the absolute vacuum level[56] are plotted in Figure 5. For the *P*1 polymorph, the CBM is 0.66 eV higher than the $H^+/H_2$ reduction potential at pH = 0, so photogenerated electrons have strong reducing ability and will produce hydrogen from water. At the same time, the VBM is 0.36 eV lower than the $H_2O/O_2$ oxidation potential at pH = 0, making photogenerated holes oxidize water to produce oxygen. Shifting the pH into neutrality will also shift the redox potentials upward, and at pH = 7, the *P*1 polymorph will remain active. For the *P*3 polymorph, the CBM is 1.39 and 0.99 eV higher than the $H^+/H_2$ reduction potential at pH = 0 and 7, respectively, highly favorable for producing hydrogen from water. On the other side, the VBM is significantly higher than the $H_2O/O_2$ oxidation potential at either pH = 0 or 7. Nonetheless, one may apply an external bias voltage or modify the *P*3 band gap by substitution to induce water oxidation.

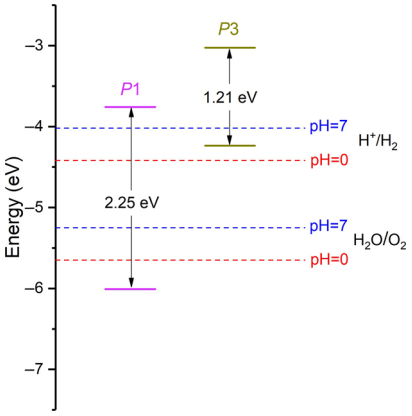


**Figure 5.** Calculated band-edge positions of $WC_3N_6$ relative to the absolute vacuum level. Redox potentials for water splitting at pH = 0 and 7 are shown for comparison.

The absorption spectra of $WC_3N_6$ were calculated using the HSE06 + RPA method and are depicted in Figure 6. The first absorption peaks of the *P*1 and *P*3 polymorphs locate at about 2.70 and 1.44 eV, respectively, close to their direct band gaps, and they are significantly smaller than that of g-$C_3N_4$ (3.7 eV) and also one of the theoretically predicted $C_3N_6$ nanosheets (4.37 eV),[11] hence ideal for the preparation of optoelectronic devices in the visible range. Moreover, the optical absorption coefficients of *P*1 and *P*3 at 300 nm are approximately as high as $4 \times 10^5$ and $3 \times 10^5$ $cm^{-1}$, respectively, several times larger than those of g-$C_3N_4$ and $C_3N_6$ nanosheets.[11] Therefore, $WC_3N_6$ does exhibit potential in the practical applications of high-efficiency optoelectronics.

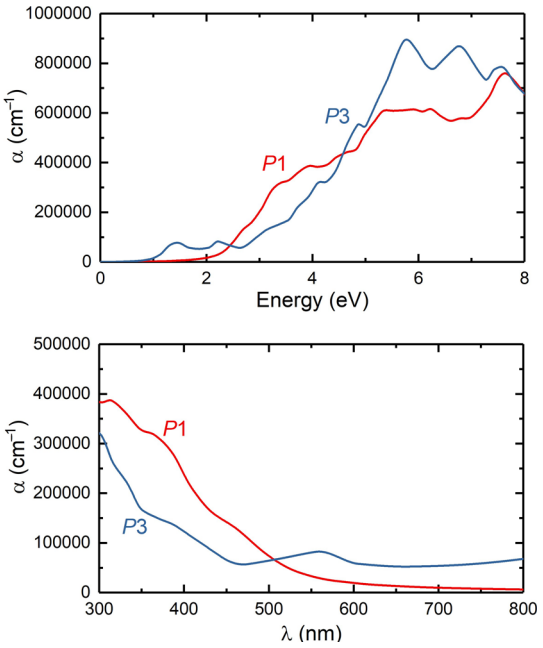


**Figure 6.** Calculated optical absorption spectra ($\alpha$) of the *P*1 and *P*3 polymorphs by the HSE06 + RPA approach (top) and their optical absorption spectra as a function of the wavelength (bottom, the visible light ranges from 380 to 750 nm).

In structural terms, we have already alluded to the porous nature of the *P*1 and *P*3 polymorphs; in case that also translates into a sufficiently large specific surface area and open channels, this could improve their ability of transporting matter and harvesting photons. In addition, the layered, hence anisotropic crystal structures of $WC_3N_6$, should allow for internal electric fields, a favorable property for the separation and transfer of photogenerated electron−hole pairs, thus enhancing the photocatalytic activities.[78] In terms of the electronic structure, unlike g-$C_3N_4$, whose molecule-like excitation is highly confined to triazine units, thus requiring a large activation energy and resulting in a low carrier separation rate,[79] the excited electron of $WC_3N_6$ will mostly go from nitrogen 2p to a tungsten 5d orbital for the *P*1 phase which should effectively increase the separation rate of the electron−hole pairs. On the other hand, the indirect band gap of $WC_3N_6$ facilitates the separation of photogenerated electron−hole pairs since excited electrons must travel a certain *k*-space distance within the conduction band before returning to the valence band, also reducing the probability of photogenerated electron−hole recombination.[78,80−82] In summary, $WC_3N_6$ should exhibit potential in photocatalysis and optoelectronic devices.

After synthesis, future experimental research on $WC_3N_6$ may address adsorption sites for molecules for various applications. Because of the porous structure, $WC_3N_6$ may be tried as a structural host for batteries.


https://doi.org/10.1021/jacs.3c00631
J. Am. Chem. Soc. XXXX, XXX, XXX−XXX

## CONCLUSIONS

We have predicted the synthetic conditions and crystal structures of two $WC_3N_6$ polymorphs adopting the *P*1 and *P*3 space groups. Both melaminate phases containing complex $C_3N_6^{6-}$ anions form layer-like porous structures with layers connected by W−N bonds and fivefold (*P*1) and sixfold (*P*3) tungsten coordination. In addition to significant ionicity, COHP chemical-bonding analysis indicates sizable covalency without antibonding, the *P*1 polymorph being less covalent than *P*3. Both *P*1 and *P*3 polymorphs are indirect semiconductors with gaps of 2.25 and 1.21 eV, respectively, making them favorable for practical applications in electronic devices. In addition, both have suitable band-edge potentials for water splitting. The CBM of *P*1 is 0.66 eV (0.25 eV) higher than the $H^+/H_2$ energy level at pH = 0 (7), while its VBM is 0.36 eV (0.77 eV) lower than the $H_2O/O_2$ energy level at pH = 0 (7), so there is driving force for overall water splitting, either in the acidic or neutral environment. As for *P*3, its CBM is 1.39 eV (0.99 eV) higher than the $H^+/H_2$ energy level at pH = 0 (7); hence, it is highly favorable for photocatalytic water reduction. As for the photoelectronic transition between VBM and CBM, the very small overlap between nitrogen 2p to tungsten 5d orbitals for the *P*1 phase suggests favorable charge-carrier transport due to reduced electron−hole recombination. In terms of optical absorption, the first absorption peaks of *P*1 and *P*3 locate at 2.7 and 1.35 eV, respectively, and their optical absorption coefficients are as high as $4 \times 10^5$ and $3 \times 10^5$ $cm^{-1}$ at 300 nm, thus improving the photocatalytic performance.

## ASSOCIATED CONTENT

### Supporting Information

The Supporting Information is available free of charge at https://pubs.acs.org/doi/10.1021/jacs.3c00631.

Density of phonon states and molecular dynamics diagrams; relative enthalpy of $WC_3N_6$ against competing phases; electronic DOS; fatbands; influence of spin-orbit coupling; crystallographic parameters; band gap values; and Löwdin atomic charges (PDF)

## AUTHOR INFORMATION


### Corresponding Author

**Richard Dronskowski** − *Chair of Solid-State and Quantum Chemistry, Institute of Inorganic Chemistry, RWTH Aachen University, D-52056 Aachen, Germany; Hoffmann Institute of Advanced Materials, Shenzhen Polytechnic, 518055 Shenzhen, China;* orcid.org/0000-0002-1925-9624; Email: drons@HAL9000.ac.rwth-aachen.de

### Authors

**Da Chen** − *Hoffmann Institute of Advanced Materials, Shenzhen Polytechnic, 518055 Shenzhen, China; Chair of Solid-State and Quantum Chemistry, Institute of Inorganic Chemistry, RWTH Aachen University, D-52056 Aachen, Germany*

**YiXu Wang** − *Chair of Solid-State and Quantum Chemistry, Institute of Inorganic Chemistry, RWTH Aachen University, D-52056 Aachen, Germany*

Complete contact information is available at: https://pubs.acs.org/10.1021/jacs.3c00631


### Notes

The authors declare no competing financial interest.

## ACKNOWLEDGMENTS

It is a pleasure to thank Professor Martin Jansen (Stuttgart) for sharing his expertise in carbon nitride chemistry. D.C. is grateful to Dr. David Schnieders, Dr. Michal Fečík, Jan Hempelmann, and Peter C. Müller for technical support regarding the computing server and useful discussions on the calculations, as well as to Dr. Alex Corkett for language assistance. Y.X.W. gratefully acknowledges the financial support from the Alexander von Humboldt Foundation.

## REFERENCES


(1) Liu, A. Y.; Cohen, M. L. Prediction of new low compressibility solids. *Science* **1989**, *245*, 841.

(2) Niu, C.; Lu, Y. Z.; Lieber, C. M. Experimental realization of the covalent solid carbon nitride. *Science* **1993**, *261*, 334.

(3) Hughbanks, T.; Tian, Y. On the structure and composition of carbon nitride. *Solid State Commun.* **1995**, *96*, 321.

(4) Jockisch, A.; Schier, A.; Schmidbaur, H. Tetra (amino) methanes: Implications of Their Structure and Reactivity Pattern for Hypothetical Carbon Nitride Frameworks. *Chem. Ber.* **1997**, *130*, 1739.

(5) Teter, D. M.; Hemley, R. J. Low-compressibility carbon nitrides. *Science* **1996**, *271*, 53.

(6) Riedel, R.; Wiehl, L.; Zerr, A.; Zinin, P.; Kroll, P. In *Superhard Materials, in Handbook of Solid State Chemistry*; Dronskowski, R., Kikkawa, S., Stein, A., Eds.; Wiley-VCH: Weinheim, New York, 2017; Vol. *6*, pp 175−200.

(7) Wang, X.; Maeda, K.; Thomas, A.; Takanabe, K.; Xin, G.; Carlsson, J. M.; Domen, K.; Antonietti, M. A metal-free polymeric photocatalyst for hydrogen production from water under visible light. *Nat. Mater.* **2009**, *8*, 76.

(8) Schmidt, C. L.; Nuss, J.; Jansen, M. Methylammonium dicyanamide: Synthesis, characterisation, and screening its potential as a precursor for $C_3N_4$ and as an ionic liquid. *Solid State Sci.* **2020**, *107*, No. 106347.

(9) Ong, W.-J.; Tan, L.-L.; Ng, Y. H.; Yong, S.-T.; Chai, S.-P. Graphitic carbon nitride (g-$C_3N_4$)-based photocatalysts for artificial photosynthesis and environmental remediation: are we a step closer to achieving sustainability? *Chem. Rev.* **2016**, *116*, 7159.

(10) Kroke, E.; Schwarz, M.; Horath-Bordon, E.; Kroll, P.; Noll, B.; Norman, A. D. Tri-s-triazine derivatives. Part I. From trichloro-tri-s-triazine to graphitic $C_3N_4$ structures. *New J. Chem.* **2002**, *26*, 508.

(11) Mortazavi, B.; Shojaei, F.; Shahrokhi, M.; Azizi, M.; Rabczuk, T.; Shapeev, A. V.; Zhuang, X. Nanoporous $C_3N_4$, $C_3N_5$ and $C_3N_6$ nanosheets; novel strong semiconductors with low thermal conductivities and appealing optical/electronic properties. *Carbon* **2020**, *167*, 40.

(12) Liu, J. Effect of phosphorus doping on electronic structure and photocatalytic performance of g-$C_3N_4$: insights from hybrid density functional calculation. *J. Alloys Compd.* **2016**, *672*, 271.

(13) Chen, Z.; Savateev, A.; Pronkin, S.; Papaefthimiou, V.; Wolff, C.; Willinger, M. G.; Willinger, E.; Neher, D.; Antonietti, M.; Dontsova, D. "The easier the better" preparation of efficient photocatalysts—metastable poly (heptazine imide) salts. *Adv. Mater.* **2017**, *29*, No. 1700555.

(14) Savateev, A.; Pronkin, S.; Willinger, M. G.; Antonietti, M.; Dontsova, D. Towards organic zeolites and inclusion catalysts: Heptazine imide salts can exchange metal cations in the solid state. *Chem. − Asian J.* **2017**, *12*, 1517.

(15) Schlomberg, H.; Kröger, J.; Savasci, G.; Terban, M. W.; Bette, S.; Moudrakovski, I.; Duppel, V.; Podjaski, F.; Siegel, R.; Senker, J.; Dinnebier, R. E.; Ochsenfeld, C.; Lotsch, B. V. Structural insights into poly (heptazine imides): a light-storing carbon nitride material for dark photocatalysis. *Chem. Mater.* **2019**, *31*, 7478.

(16) McDermott, E. J.; Wirnhier, E.; Schnick, W.; Virdi, K. S.; Scheu, C.; Kauffmann, Y.; Kaplan, W. D.; Kurmaev, E. Z.; Moewes, A.

Band gap tuning in poly (triazine imide), a nonmetallic photocatalyst. *J. Phys. Chem. C* **2013**, *117*, 8806.
(17) Banerjee, T.; Podjaski, F.; Kröger, J.; Biswal, B. P.; Lotsch, B. V. Polymer photocatalysts for solar-to-chemical energy conversion. *Nat. Rev. Mater.* **2021**, *6*, 168.
(18) Gao, H.; Yan, S.; Wang, J.; Huang, Y. A.; Wang, P.; Li, Z.; Zou, Z. Towards efficient solar hydrogen production by intercalated carbon nitride photocatalyst. *Phys. Chem. Chem. Phys.* **2013**, *15*, 18077.
(19) Chen, K.; Fehse, M.; Laurita, A.; Arayamparambil, J. J.; Sougrati, M. T.; Stievano, L.; Dronskowski, R. Quantum-Chemical Study of the FeNCN Conversion-Reaction Mechanism in Lithium- and Sodium-Ion Batteries. *Angew. Chem., Int. Ed.* **2020**, *59*, 3718.
(20) Tang, X.; Xiang, H.; Liu, X.; Speldrich, M.; Dronskowski, R. A ferromagnetic carbodiimide: $Cr_2(NCN)_3$. *Angew. Chem., Int. Ed.* **2010**, *49*, 4738.
(21) Sougrati, M. T.; Arayamparambil, J. J.; Liu, X.; Mann, M.; Slabon, A.; Stievano, L.; Dronskowski, R. Carbodiimides as energy materials: which directions for a reasonable future? *Dalton Trans.* **2018**, *47*, 10827.
(22) Luo, D.; Yin, K.; Dronskowski, R. Existence of $BeCN_2$ and Its First-Principles Phase Diagram: Be and C Introducing Structural Diversity. *J. Am. Chem. Soc.* **2022**, *144*, 5155.
(23) Corkett, A. J.; Chen, Z.; Ertural, C.; Slabon, A.; Dronskowski, R. Synthetic Engineering in $Na_2MSn_2(NCN)_6$ (M=Mn, Fe, Co, and Ni) Based on Electronic Structure Theory. *Inorg. Chem.* **2022**, *61*, 18221.
(24) Qiao, X.; Chen, K.; Corkett, A. J.; Mroz, D.; Huang, X.; Wang, R.; Nelson, R.; Dronskowski, R. Synthesis, Crystal Structure, Symmetry Relationships, and Electronic Structure of Bismuth Carbodiimide $Bi_2(NCN)_3$ and Its Ammonia Adduct $Bi_2(NCN)_3 \cdot NH_3$. *Inorg. Chem.* **2021**, *60*, 12664.
(25) Missong, R.; George, J.; Houben, A.; Hoelzel, M.; Dronskowski, R. Synthesis, Structure, and Properties of $SrC(NH)_3$, a Nitrogen-Based Carbonate Analogue with the Trinacria Motif. *Angew. Chem., Int. Ed.* **2015**, *54*, 12171.
(26) Zhang, J.; Corkett, A. J.; van Leusen, J.; Englert, U.; Dronskowski, R. Solvent-Induced Cobalt (II) Cyanoguanidine Bromides: Syntheses, Crystal Structure, Optical and Magnetic Properties. *Crystals* **2022**, *12*, 1377.
(27) Luo, D.; Qiao, X.; Dronskowski, R. Predicting Nitrogen-Based Families of Compounds: Transition-Metal Guanidinates $TCN_3$ (T = V, Nb, Ta) and Ortho-Nitrido Carbonates $T'_2CN_4$ (T′ = Ti, Zr, Hf). *Angew. Chem., Int. Ed.* **2021**, *60*, 486.
(28) Bann, B.; Miller, S. A. Melamine and derivatives of melamine. *Chem. Rev.* **1958**, *58*, 131.
(29) Franklin, E. C. The ammono carbonic acids. *J. Am. Chem. Soc.* **1922**, *44*, 486.
(30) Schnick, W.; Huppertz, H. Darstellung, Kristallstruktur und Eigenschaften von Kaliumhydrogencyanamid. *Z. Anorg. Allg. Chem.* **1995**, *621*, 1703.
(31) Görne, A. L.; Scholz, T.; Kobertz, D.; Dronskowski, R. Deprotonating Melamine to Gain Highly Interconnected Materials: Melaminate Salts of Potassium and Rubidium. *Inorg. Chem.* **2021**, *60*, 15069.
(32) Kallenbach, P.; Bayat, E.; Ströbele, M.; Romao, C. P.; Meyer, H.-J. Tricopper Melaminate, a Metal−Organic Framework Containing Dehydrogenated Melamine and Cu−Cu Bonding. *Inorg. Chem.* **2021**, *60*, 16303.
(33) Wang, Y.; Lv, J.; Zhu, L.; Ma, Y. CALYPSO: A method for crystal structure prediction. *Comput. Phys. Commun.* **2012**, *183*, 2063.
(34) Wang, Y.; Lv, J.; Zhu, L.; Ma, Y. Crystal structure prediction via particle-swarm optimization. *Phys. Rev. B* **2010**, *82*, No. 094116.
(35) Gao, B.; Gao, P.; Lu, S.; Lv, J.; Wang, Y.; Ma, Y. Interface structure prediction via CALYPSO method. *Sci. Bull.* **2019**, *64*, 301.
(36) Oganov, A. R.; Lyakhov, A. O.; Valle, M. How Evolutionary Crystal Structure Prediction Works-and Why. *Acc. Chem. Res.* **2011**, *44*, 227.
(37) Oganov, A. R.; Glass, C. W. Crystal structure prediction using ab initio evolutionary techniques: Principles and applications. *J. Chem. Phys.* **2006**, *124*, 244704.
(38) Lyakhov, A. O.; Oganov, A. R.; Stokes, H. T.; Zhu, Q. New developments in evolutionary structure prediction algorithm USPEX. *Comput. Phys. Commun.* **2013**, *184*, 1172.
(39) Oganov, A. R.; Pickard, C. J.; Zhu, Q.; Needs, R. J. Structure prediction drives materials discovery. *Nat. Rev. Mater.* **2019**, *4*, 331.
(40) Zhang, L.; Wang, Y.; Lv, J.; Ma, Y. Materials discovery at high pressures. *Nat. Rev. Mater.* **2017**, *2*, 17005.
(41) Perdew, J. P.; Burke, K.; Ernzerhof, M. Generalized gradient approximation made simple. *Phys. Rev. Lett.* **1996**, *77*, 3865.
(42) Grimme, S.; Antony, J.; Ehrlich, S.; Krieg, H. A consistent and accurate ab initio parametrization of density functional dispersion correction (DFT-D) for the 94 elements H-Pu. *J. Chem. Phys.* **2010**, *132*, 154104.
(43) Grimme, S.; Ehrlich, S.; Goerigk, L. Effect of the damping function in dispersion corrected density functional theory. *J. Comput. Chem.* **2011**, *32*, 1456.
(44) Kresse, G.; Furthmüller, J. Efficiency of ab-initio total energy calculations for metals and semiconductors using a plane-wave basis set. *Comput. Mater. Sci.* **1996**, *6*, 15.
(45) Kresse, G.; Furthmüller, J. Efficient iterative schemes for ab initio total-energy calculations using a plane-wave basis set. *Phys. Rev. B* **1996**, *54*, 11169.
(46) Kresse, G.; Hafner, J. Ab initio molecular dynamics for liquid metals. *Phys. Rev. B* **1993**, *47*, 558.
(47) Kresse, G.; Hafner, J. Ab initio molecular-dynamics simulation of the liquid-metal−amorphous-semiconductor transition in germanium. *Phys. Rev. B* **1994**, *49*, 14251.
(48) Blöchl, P. E. Projector augmented-wave method. *Phys. Rev. B* **1994**, *50*, 17953.
(49) Kresse, G.; Joubert, D. From ultrasoft pseudopotentials to the projector augmented-wave method. *Phys. Rev. B* **1999**, *59*, 1758.
(50) Anisimov, V. I.; Zaanen, J.; Andersen, O. K. Band theory and Mott insulators: Hubbard *U* instead of Stoner *I*. *Phys. Rev. B* **1991**, *44*, 943.
(51) Solovyev, I. V.; Dederichs, P. H.; Anisimov, V. I. Corrected atomic limit in the local-density approximation and the electronic structure of d impurities in Rb. *Phys. Rev. B* **1994**, *50*, 16861.
(52) Hurtado-Aular, O.; Añez, R.; Sierraalta, A. DFT+*U* study of the electronic structure changes of $WO_3$ monoclinic and hexagonal surfaces upon Cu, Ag, and Au adsorption. Applications for CO adsorption. *Surf. Sci.* **2021**, *714*, No. 121907.
(53) Qi, T.; Grinberg, I.; Rappe, A. M. Band-gap engineering via local environment in complex oxides. *Phys. Rev. B* **2011**, *83*, No. 224108.
(54) Krukau, A. V.; Vydrov, O. A.; Izmaylov, A. F.; Scuseria, G. E. Influence of the exchange screening parameter on the performance of screened hybrid functionals. *J. Chem. Phys.* **2006**, *125*, 224106.
(55) Praus, P. On electronegativity of graphitic carbon nitride. *Carbon* **2021**, *172*, 729.
(56) Li, Y.; Li, Y.-L.; Araujo, C. M.; Luo, W.; Ahuja, R. Single-layer $MoS_2$ as an efficient photocatalyst. *Catal. Sci. Technol.* **2013**, *3*, 2214.
(57) Maintz, S.; Deringer, V. L.; Tchougréeff, A. L.; Dronskowski, R. Analytic projection from plane-wave and PAW wavefunctions and application to chemical-bonding analysis in solids. *J. Comput. Chem.* **2013**, *34*, 2557.
(58) Maintz, S.; Deringer, V. L.; Tchougréeff, A. L.; Dronskowski, R. LOBSTER: A Tool to Extract Chemical Bonding from Plane-Wave Based DFT. *J. Comput. Chem.* **2016**, *37*, 1030.
(59) Nelson, R.; Ertural, C.; George, J.; Deringer, V. L.; Hautier, G.; Dronskowski, R. LOBSTER: Local orbital projections, atomic charges, and chemical-bonding analysis from projector-augmented-wave-based density-functional theory. *J. Comput. Chem.* **2020**, *41*, 1931.
(60) Dronskowski, R.; Blöchl, P. E. Crystal orbital Hamilton populations (COHP): energy-resolved visualization of chemical


https://doi.org/10.1021/jacs.3c00631
J. Am. Chem. Soc. XXXX, XXX, XXX−XXX

bonding in solids based on density-functional calculations. *J. Phys. Chem.* **1993**, *97*, 8617.
(61) Deringer, V. L.; Tchougréeff, A. L.; Dronskowski, R. Crystal orbital Hamilton population (COHP) analysis as projected from plane-wave basis sets. *J. Phys. Chem. A* **2011**, *115*, 5461.
(62) Müller, P. C.; Ertural, C.; Hempelmann, J.; Dronskowski, R. Crystal orbital bond index: covalent bond orders in solids. *J. Phys. Chem. C* **2021**, *125*, 7959.
(63) Wang, V.; Xu, N.; Liu, J.-C.; Tang, G.; Geng, W.-T. VASPKIT: A user-friendly interface facilitating high-throughput computing and analysis using VASP code. *Comput. Phys. Commun.* **2021**, *267*, No. 108033.
(64) Momma, K.; Izumi, F. VESTA 3 for three-dimensional visualization of crystal, volumetric and morphology data. *J. Appl. Crystallogr.* **2011**, *44*, 1272.
(65) Holleman, A.; Wiberg, E.; Wiberg, N. *Lehrbuch der Anorganischen Chemie*, 102nd ed.; De Gruyter: Berlin, Germany, 2007.
(66) Van Santen, R. A. The Ostwald step rule. *J. Phys. Chem.* **1984**, *88*, 5768.
(67) Shannon, R. D. Revised effective ionic radii and systematic studies of interatomic distances in halides and chalcogenides. *Acta Crystallogr., Sect. A* **1976**, *32*, 751.
(68) Diehl, R.; Brandt, G.; Salje, E. The crystal structure of triclinic $WO_3$. *Acta Crystallogr., Sect. B: Struct. Sci., Cryst. Eng. Mater.* **1978**, *34*, 1105.
(69) Larson, A. C.; Cromer, D. T. Crystal structure refinements with generalized scattering factors. II. Melamine, 2, 4, 6-triamino-s-triazine. *J. Chem. Phys.* **1974**, *60*, 185.
(70) Kuhs, W. F.; Lehmann, M. S. The structure of the ice Ih by neutron diffraction. *J. Phys. Chem.* **1983**, *87*, 4312.
(71) Chase, M. W., Jr.; NIST-JANAF Thermochemical Tables, Fourth Edition, *J. Phys. Chem. Ref. Data*, Monograph 9, 1998.
(72) Hughes, E. W. The crystal structure of melamine. *J. Am. Chem. Soc.* **1941**, *63*, 1737.
(73) Biltz, W. *Raumchemie der festen Stoffe*; Verlag von Leopold Voss: Leipzig, 1934.
(74) Wang, F.; Di Valentin, C. D.; Pacchioni, G. Electronic and structural properties of $WO_3$: a systematic hybrid DFT study. *J. Phys. Chem. C* **2011**, *115*, 8345.
(75) Ma, X.; Lv, Y.; Xu, J.; Liu, Y.; Zhang, R.; Zhu, Y. A strategy of enhancing the photoactivity of g-$C_3N_4$ via doping of nonmetal elements: a first-principles study. *J. Phys. Chem. C* **2012**, *116*, 23485.
(76) Peng, B. Monolayer fullerene networks as photocatalysts for overall water splitting. *J. Am. Chem. Soc.* **2022**, *144*, 19921.
(77) Chakrapani, V.; Angus, J. C.; Anderson, A. B.; Wolter, S. D.; Stoner, B. R.; Sumanasekera, G. U. Charge transfer equilibria between diamond and an aqueous oxygen electrochemical redox couple. *Science* **2007**, *318*, 1424.
(78) Zhang, K.-L.; Liu, C.-M.; Huang, F.-Q.; Zheng, C.; Wang, W.-D. Study of the electronic structure and photocatalytic activity of the BiOCl photocatalyst. *Appl. Catal., B* **2006**, *68*, 125.
(79) Liu, F.; Tong, Y.; Li, C.; Liu, X. One-Dimensional Conjugated Carbon Nitrides: Synthesis and Structure Determination by HRTEM and Solid-State NMR. *J. Phys. Chem. Lett.* **2021**, *12*, 10359.
(80) Amtout, A.; Leonelli, R. Optical properties of rutile near its fundamental band gap. *Phys. Rev. B* **1995**, *51*, 6842.
(81) Asahi, R.; Taga, Y.; Mannstadt, W.; Freeman, A. J. Electronic and optical properties of anatase $TiO_2$. *Phys. Rev. B* **2000**, *61*, 7459.
(82) Glassford, K. M.; Chelikowsky, J. R. Structural and electronic properties of titanium dioxide. *Phys. Rev. B* **1992**, *46*, 1284.




https://doi.org/10.1021/jacs.3c00631
J. Am. Chem. Soc. XXXX, XXX, XXX−XXX